ACADEMIC PRESS

Journal of Solid State Chemistry 169 (2002) 44–52

JOURNAL OF SOLID STATE CHEMISTRY

www.academicpress.com

Cation ordering in $Li_2M(II)Sn_3O_8$, $M(II) = Mn,\ Zn$

D. Kovacheva,[a,*] T. Trendafilova,[a] K. Petrov,[a] and A. Hewat[b]

[a] *Institute of General and Inorganic Chemistry, Bulgarian Academy of Sciences, Acad. G. Bonchev Street, bl.11, 1113 Sofia, Bulgaria*
[b] *Institute Laue-Langevin, Grenoble, BP 156, F-38042 Grenoble Cedex 9, France*

Received 5 March 2002; received in revised form 14 June 2002; accepted 20 August 2002

Abstract

New complex oxides with general formula $Li_2M(II)Sn_3O_8$ ($M = Mn,\ Zn$) have been synthesized and studied by powder neutron diffraction. They crystallize in the orthorhombic system, space group $Cmc2_1$, $Z = 12$. For $Li_2MnSn_3O_8$, the lattice constants obtained from the refinement are $a = 18.3795(6)$, $b = 10.6080(3)$; $c = 9.90056(6)$ Å; for $Li_2ZnSn_3O_8$, $a = 18.2048(8)$, $b = 10.5098(5)$ and $c = 9.87158(7)$ Å. The structure consists of a hexagonal close packed array of oxygen layers stacked along $\langle c \rangle$ direction in a sequence (ABCB) in which cations occupy 1/8 of the tetrahedral and 1/2 of the octahedral interstices. The structure can be derived from that of the partially disordered $LiFeSnO_4$ (space group $P6_3mc$) described earlier, assuming complete cation ordering. The influence of two antagonistic factors that govern the cation distribution (the electrostatic repulsion between the adjacent high valence cations and the geometrical factor, that accounts for the ionic size) is discussed.

Keywords: Cation ordering; Double-hexagonal phases; Superstructure; Neutron diffraction

1. Introduction

Structural studies of lithium-containing complex metal oxides have gained much interest because of their contribution to better understanding of important physical properties, such as electronic and ionic transport, reversible lithium intercalation, electrochemical sensing, etc. Oxides with general formula $Li_{2x}M_{4-3x}Sn_{2+x}O_8$ ($M = Zn,\ Mg$), $(0.67 < x < 1.0)$ comprise a group of quaternary compounds formed on the join M_2SnO_4—hypothetical $Li_4Sn_5O_{12}$ of the phase diagram Li_2O–MO–SnO_2. The structure of these phases represents a double-hexagonal (DH) array of four oxygen layers, stacked along the $\langle c \rangle$ direction in a sequence ABAC. Cations occupy the octahedral—6(*c*) and 2(*b*) and the tetrahedral—2(*a*) and 2(*b*) lattice sites of the space group $P6_3mc$ [1]. This structure is tolerant with respect to isomorphic cationic substitutions. Successful synthesis of many members of the same structural type, containing large number of other iso- or aliovalent cations such as Fe^{3+}, Sb^{5+}, Cr^{3+}, Al^{3+}, Ga^{3+}, Cu^{2+}, Ti^{4+} was reported [1–4]. The DH structure is stable at temperatures between 800°C and 1100°C. At higher temperatures (1200–1300°C) it transforms reversibly to ramsdellite [2,4,5] or spinel-type [3,6] structure. Recently, a reversible transformation between the spinel $LiMn_2O_4$ and the DH $Li_{1-x}Mn_2O_4$ was reported. It clarified the anomalies of the potential-composition profiles of $LiMn_2O_4$ cathode materials upon lithium extraction/reinsertion [7].

It is well known that practically all the physical and chemical properties of the metal oxide materials are directly related to their elemental composition, crystal structure and cationic distribution. All these phases exhibit mixed occupancies of the 6(*c*) lattice sites as a rule. In some of them, the rest of the lattice sites are occupied by individual atoms: Li: 2(*a*), Zn: 2(*b*) and Sn: 2(*b*) in $Li_{1.6}Zn_{1.6}Sn_{2.8}O_8$; Li: 2(*a*), Mg: 2(*b*) and Sn: 2(*b*) in $Li_{1.6}Mg_{1.6}Sn_{2.8}O_8$ [1]; Li: 2(*a*), 2(*b*) and Sb: 2(*b*) in $Li_2Cr_2AlSbO_8$, $Li_2Cr_2FeSbO_8$ and $Li_2CrAl_2SbO_8$ [3]; Mixed occupancy (Li,Fe) in the 2(*b*) tetrahedral site was observed for $LiFeSnO_4$ [2,4], while $Li_2Fe_3SbO_8$ exhibits mixed occupancies of the 2(*a*) and 2(*b*) tetrahedral and the 2(*b*) octahedral lattice sites [3]. One can hardly expect that this disorder is inherent to the particular structural type. It could be rather compositionally and geometrically conditioned.

*Corresponding author. Fax: +359-2-70-50-24.
E-mail address: didka@svr.igic.bas.bg (D. Kovacheva).

0022-4596/02/$ - see front matter
PII: S0022-4596(02)00015-4

In the present paper, we report the synthesis and structural characteristics of two new compounds—$Li_2ZnSn_3O_8$ and $Li_2MnSn_3O_8$ that, contrary to the mentioned disordered phases, exhibit complete cation ordering.

2. Experimental

The samples of $Li_2ZnSn_3O_8$ and $Li_2MnSn_3O_8$ were synthesized by solid state reaction between Li_2CO_3, ZnO or Mn(II) oxalate, and SnO_2. Li_2CO_3 and ZnO were commercial products of analytical grade purity. Mn(II) oxalate—$Mn(COO)_2 . 2H_2O$ was precipitated by adding an excess of concentrated solution of oxalic acid to 0.2 M solution of $KMnO_4$. The white crystalline precipitate was filtered, washed with distilled water and dried at 60°C in air. The freshly prepared SnO_2 with high specific surface and enhanced reactivity was obtained by dissolving metal tin of 99.999% purity (United Min. and Chem. Corp.) in dilute nitric acid. Stannic acid was precipitated from the clear solution upon boiling. The precipitate was washed continuously until neutral reaction and heated at 400°C for 3 h.

A 15 g sample of $Li_2ZnSn_3O_8$ for neutron diffraction studies was obtained by mixing and grinding stoichiometric amounts of the initial compounds in an agate mortar. Prior to mixing, Li_2CO_3 and ZnO were heated at 300°C for 2 h. The homogenized powder was pressed into cylindrical pellets (12 mm diameter and 5 mm high) at 430 MPa, and heated at 1000°C for 12 h in air, with one intermediate grinding. The same steps were followed to prepare a reference sample with composition $Li_{1.6}Zn_{1.6}Sn_{2.8}O_8$.

In order to prevent the oxidation of Mn^{2+}, a different preparation procedure was used to obtain a 12 g sample of $Li_2MnSn_3O_8$. Pellets of the starting reagents, prepared in the same way as that of $Li_2ZnSn_3O_8$, were deeply buried in a large volume of powdered reaction mixture placed in a corundum boat. The boat was introduced into a muffle furnace in an atmosphere of flowing argon, heated at 800°C for 2 h and annealed slowly to room temperature. The treatment was repeated at 1000°C with intermediate grinding.

X-ray powder diffraction (XRD) data, for preliminary characterization, were collected from 5° to 145° 2θ with a constant step of 0.02° 2θ and 5 s/step counting time at room temperature, on a DRON-3 automatic powder diffractometer using filtered Cu$K\alpha$ radiation.

For neutron diffraction experiments, fine powdered samples were placed in a 12 mm vanadium can. Powder patterns were collected at room temperature with a constant wavelength of 1.594 Å over the range 5–160° 2θ, with a step 0.05° 2θ, on the high-resolution neutron powder diffractometer D2B at the Institute Laue-Langevin in Grenoble, France. At each point of the diffraction pattern the counts were averaged over the different detectors.

The FULLPROF program suite [8] was used for the structural refinements. The pseudo-Voigt function defined within seven full-widths at half-maximum (FWHM) was used for approximation of the diffraction profiles. The refined instrumental and structural parameters were: zero shift, scale factor, background parameters, lattice parameters, line profile parameters, atomic positional parameters, individual isotropic displacement parameters and cation site occupancies. The scattering lengths used were: (Li) −0.190, (Sn) 0.6225, (O) 0.5803, (Mn) −0.373 and (Zn) 0.568 fm.

The infrared (IR) spectra were recorded with a Bruker IFS 25 FTI spectrometer in the range 400–4000 cm^{-1} (resolution $<2\ cm^{-1}$). The routine KBr technique of sample preparation was used. Ion exchange or other reactions between the sample and KBr were not observed.

The XPS measurements were carried out in the UHV chamber of the electron spectrometer ESCALAB MkII (VG Scientific) equipped with a Mg$K\alpha$ excitation source. The spectra calibration was performed by using C1s line of adventitious carbon, centered at 285 eV.

3. Results and discussion

The powdered $Li_2ZnSn_3O_8$ sample was white, while that of the $Li_2MnSn_3O_8$ was light yellow. Routine XRD analyses showed that the samples prepared in small batches and for shorter reaction time were single phase. Small amounts of SnO_2 impurity, coming from the protective powder coating, were detected in the batch of $Li_2MnSn_3O_8$ prepared for neutron diffraction experiments.

The XPS of the Mn $2p$ spectral region is presented in Fig. 1. The manganese photoelectron binding energies of 641.3 eV for the $2p_{3/2}$ and 653.0 eV for the $2p_{1/2}$ transitions, and especially the existence of the satellite peak at approximately 5.4 eV below the main $2p_{3/2}$ peak, evidence the presence of Mn^{2+} species only [9,10]. In particular, this explains the observed color of the sample.

According to Choisnet et al. [1], $Li_2ZnSn_3O_8$ is the end member of a series of phases with general formula $Li_{2x}M_{4-3x}Sn_{2+x}O_8$ that form in the compositional interval $0.67<x<1.0$. These phases are of DH-type and crystallize in the space group $P6_3mc$. The unit-cell parameters of the particular composition $Li_{1.6}Zn_{1.6}Sn_{2.8}O_8$ are $a_h = 6.06$ Å, $c_h = 9.88$ Å, the axial ratio $c/a = 1.63$ being very close to the ideal value (1.633) for hexagonal close packing. The cations form two distinct layers. One is Kagomé net [Oc_3] built of ($Li_{0.2}Zn_{0.2}Sn_{0.6}$) average ions with octahedral coordination. The other is [T_2Oc]. It is built of individual Li and

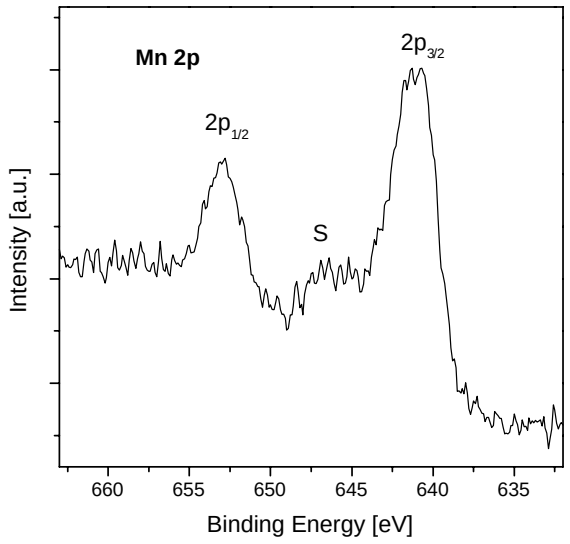

Fig. 1. XPS of the Mn 2*p* spectral region. The satellite peak is indicated by S.

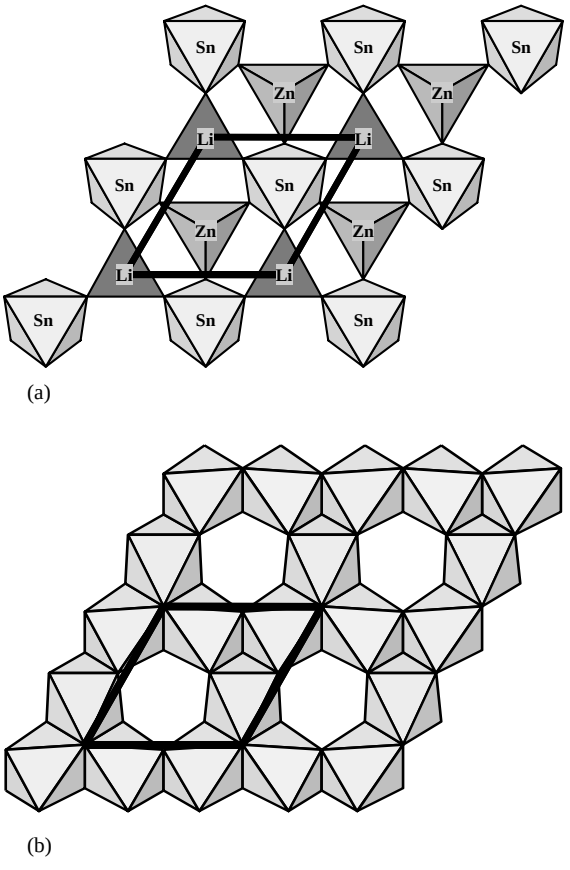

Fig. 2. Crystal structure of $Li_{1.6}Zn_{1.6}Sn_{2.8}O_8$ projected along the *c*-axis. (a) [T_2Oc] layer, (b) [Oc_3] layer formed by identical "average" $(Li_{0.2}Zn_{0.2}Sn_{0.6})O_6$ octahedra. The unit cell is outlined.

Zn in tetrahedral coordination, and Sn in octahedral coordination—see Fig. 2a and b. Contrary to the spinel structure, the octahedral vacancy in the Kagomé layer is blocked on both sides not by two occupied tetrahedra but by one octahedron and one tetrahedron.

XRD patterns of $Li_2ZnSn_3O_8$ and $Li_2MnSn_3O_8$ contain one set of diffraction lines, which are consistent with the space group and unit-cell parameters of the DH-phase described above, along with another set of additional lines (see Fig. 3). The angle positions and intensities of the latter could not be attributed unambiguously to any known impurity phases of the system. Indexing of the whole pattern of the $Li_2ZnSn_3O_8$ phase (ITO, TREOR) resulted in excellent figures of merits for two different cells: one hexagonal with $a = 10.50$ and $c = 9.87$ Å and the other C-centered orthorhombic with $a = 18.18$, $b = 10.50$ and $c = 9.87$ Å. The axial metric relations showed that both cells are super-cells of the DH-phase. The existence of a super-cell implies some kind of ordering. Therefore, splitting of the position occupied by the "average" ion of the disordered structure in two or more individual positions should be expected.

Systematic extinctions ($0\,0\,l = 2n$) for the hexagonal cell indicated possible space groups $P6_3$, $P6_322$ and $P6_3/m$. Obviously, the most plausible structural model, that accounts for the observed supercell should be similar to that of the DH-phase. The packing sequence of the oxygen layers should remain unchanged. The ordered [T_2Oc] layer in the DH-phase could not give rise to additional super-structure reflections. Therefore, the super-structure must imply cation ordering in the [Oc_3] layers. The cation content of this layer is Sn_2Li. Thus, the problem is reduced to finding an arrangement of one Li and two Sn atoms of the [Oc_3] layer in one of the three hexagonal space groups. However, none of them allows complete ordering. Nevertheless, XRD Rietveld refinements of models with partial ordering were tried. They ended with unsatisfactory fits to the data, the site occupancy factors being in drastic disagreement with the content of the formula unit. Lowering the symmetry to trigonal $P31m$ did not help.

Complete cationic ordering only became possible by further lowering the symmetry to $Cmc2_1$ which is a subgroup of $P6_3mc$. Refinements in this space group ended with tolerable values of statistical criteria, acceptable bond lengths and site occupancy factors for the heavy Zn, Mn and Sn atoms. Because of the low values of the atomic scattering factors of the light atoms and the large number of variable parameters, the positional and displacement parameters of the lithium and oxygen atoms were determined with relatively high standard deviations. These results were used as a starting model for structure refinement of the neutron diffraction data.

Tables 1 and 2 contain the final refinement parameters of the two samples. The fitted neutron diffraction patterns are shown in Figs. 4 and 5. Table 3 gives selected metal–oxygen distances and corresponding

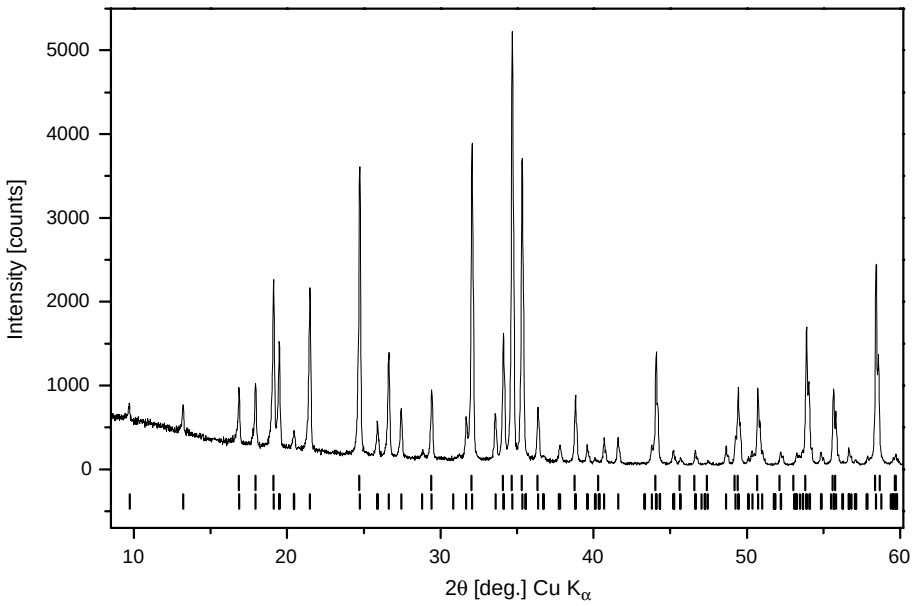

Fig. 3. XRD pattern of $Li_2ZnSn_3O_8$. Upper set of tick marks below the pattern indicates Bragg positions for the disordered ($P6_3mc$) $Li_{1.6}Zn_{1.6}Sn_{2.8}O_8$ phase. Lower set of tick marks shows Bragg positions for the ordered ($Cmc2_1$) phase.

Table 1
Refined structural parameters for $Li_2MnSn_3O_8$

Space group	a (Å)		b (Å)	c (Å)		Z
$Cmc2_1$ (No.36)	18.3795(6)		10.6080(3)	9.90056(6)		12
Atom	Wyck.	x/a	y/b	z/c	B_{iso} (Å^2)	SOF
Sn(1)	8*b*	0.0877(6)	0.0733(8)	0[a]	0.32(3)	1.000
Sn(2)	8*b*	0.0860(4)	0.5926(8)	−0.003(1)	0.32(3)	1.000
Sn(3)	8*b*	0.1708(4)	0.335(1)	−0.003(2)	0.32(3)	1.000
Li(1)	8*b*	0.251(1)	0.085(2)	0.004(3)	1.4(2)	1.000
Li(2)	4*a*	0	0.836(2)	0.001(3)	1.4(2)	1.000
Li(3)	4*a*	0	0.016(3)	0.290(2)	1.2(2)	1.000
Li(4)	8*b*	0.1836(9)	0.479(2)	0.279(2)	1.2(2)	1.000
Mn(1)	4*a*	0	0.334(4)	0.190(1)	0.83(8)	1.000
Mn(2)	8*b*	0.166(2)	0.838(2)	0.185(1)	0.83(8)	1.000
Sn(4)	4*a*	0	0.671(2)	0.282(1)	0.34(6)	1.000
Sn(5)	8*b*	0.1679(8)	0.170(1)	0.277(1)	0.34(6)	1.000
O(1)	4*a*	0	0.161(2)	−0.114(2)	0.59(2)	1.000
O(2)	8*b*	0.0850(9)	−0.081(1)	−0.121(2)	0.59(2)	1.000
O(3)	4*a*	0	0.664(2)	−0.107(1)	0.59(2)	1.000
O(4)	8*b*	0.0837(8)	0.420(2)	−0.116(2)	0.59(2)	1.000
O(5)	8*b*	0.2476(8)	0.413(2)	−0.125(1)	0.59(2)	1.000
O(6)	8*b*	0.1633(9)	0.670(1)	−0.113(1)	0.59(2)	1.000
O(7)	8*b*	0.1645(9)	0.170(2)	−0.107(1)	0.59(2)	1.000
O(8)	4*a*	0	0.008(1)	0.097(2)	0.43(3)	1.000
O(9)	4*a*	0	0.522(2)	0.124(2)	0.43(3)	1.000
O(10)	8*b*	0.0936(7)	0.240(1)	0.123(2)	0.43(3)	1.000
O(11)	8*b*	0.0754(6)	0.735(1)	0.142(2)	0.43(3)	1.000
O(12)	8*b*	0.1650(8)	0.020(1)	0.135(2)	0.43(3)	1.000
O(13)	8*b*	0.2380(8)	0.2565(8)	0.138(2)	0.43(3)	1.000
O(14)	8*b*	0.1636(6)	0.501(1)	0.097(1)	0.43(3)	1.000

[a] Determines origin. $R_P = 7.27$, $R_{wP} = 8.21$, $R_B = 2.27$, $R_F = 1.87$, $\chi^2 = 3.61$.

calculated bond valence sums (BVS). The $Li_2MnSn_3O_8$ unit-cell parameters are higher than the corresponding ones for $Li_2ZnSn_3O_8$. This fact is not only due to the larger tetrahedral ionic radius of Mn^{2+} (0.66) compared to that of Zn^{2+}(0.60) [11], but also to the larger lithium–oxygen distances of Li(1) and Li(2) in the [Oc_3] layers.

Table 2
Refined structural parameters for $Li_2ZnSn_3O_8$

Space group	a (Å)		b (Å)	c (Å)		Z
$Cmc2_1$ (No.36)	18.2048(8)		10.5098(5)	9.87158(7)		12
Atom	Wyck.	x/a	y/b	z/c	B_{iso} (Å^2)	SOF
Sn(1)	8*b*	0.0875(6)	0.0715(9)	0[a]	0.31(4)	1.000
Sn(2)	8*b*	0.0856(4)	0.5927(9)	0.001(2)	0.31(4)	1.000
Sn(3)	8*b*	0.1726(4)	0.334(1)	0.004(2)	0.31(4)	1.000
Li(1)	8*b*	0.249(2)	0.082(3)	0.007(3)	1.3(4)	0.93(1)Li0.07(1)Zn
Li(2)	4*a*	0	0.836(3)	0.010(4)	1.3(4)	0.88(2)Li0.12(2)Zn
Li(3)	4*a*	0	0.032(3)	0.293(3)	1.4(3)	1.000
Li(4)	8*b*	0.182(1)	0.481(3)	0.279(2)	1.4(3)	1.000
Zn(1)	4*a*	0	0.331(4)	0.190(1)	0.39(5)	0.88(1)Zn 0.12(1)Li
Zn(2)	8*b*	0.167(1)	0.831(2)	0.193(1)	0.39(5)	0.987(8)Zn 0.013(8)Li
Sn(4)	4*a*	0	0.669(3)	0.283(1)	0.37(6)	1.000
Sn(5)	8*b*	0.168(1)	0.168(2)	0.281(1)	0.37(6)	1.000
O(1)	4*a*	0	0.159(2)	−0.108(2)	0.44(3)	1.000
O(2)	8*b*	0.0834(7)	−0.078(1)	−0.121(2)	0.44(3)	1.000
O(3)	4*a*	0	0.664(3)	−0.105(2)	0.44(3)	1.000
O(4)	8*b*	0.0825(8)	0.420(1)	−0.111(2)	0.44(3)	1.000
O(5)	8*b*	0.2490(9)	0.415(2)	−0.119(1)	0.44(3)	1.000
O(6)	8*b*	0.1651(7)	0.670(1)	−0.108(1)	0.44(3)	1.000
O(7)	8*b*	0.165(1)	0.171(2)	−0.103(1)	0.44(3)	1.000
O(8)	4*a*	0	0.007(2)	0.108(2)	0.42(2)	1.000
O(9)	4*a*	0	0.520(2)	0.135(2)	0.42(2)	1.000
O(10)	8*b*	0.0918(7)	0.241(2)	0.128(1)	0.42(2)	1.000
O(11)	8*b*	0.0773(8)	0.738(2)	0.141(2)	0.42(2)	1.000
O(12)	8*b*	0.1648(9)	0.014(2)	0.139(2)	0.42(2)	1.000
O(13)	8*b*	0.2389(8)	0.251(1)	0.147(1)	0.42(2)	1.000
O(14)	8*b*	0.1653(7)	0.500(2)	0.100(2)	0.42(2)	1.000

[a] Determines origin. $R_P = 6.29$, $R_{wP} = 7.36$, $R_B = 2.19$, $R_F = 1.78$, $\chi^2 = 3.03$.

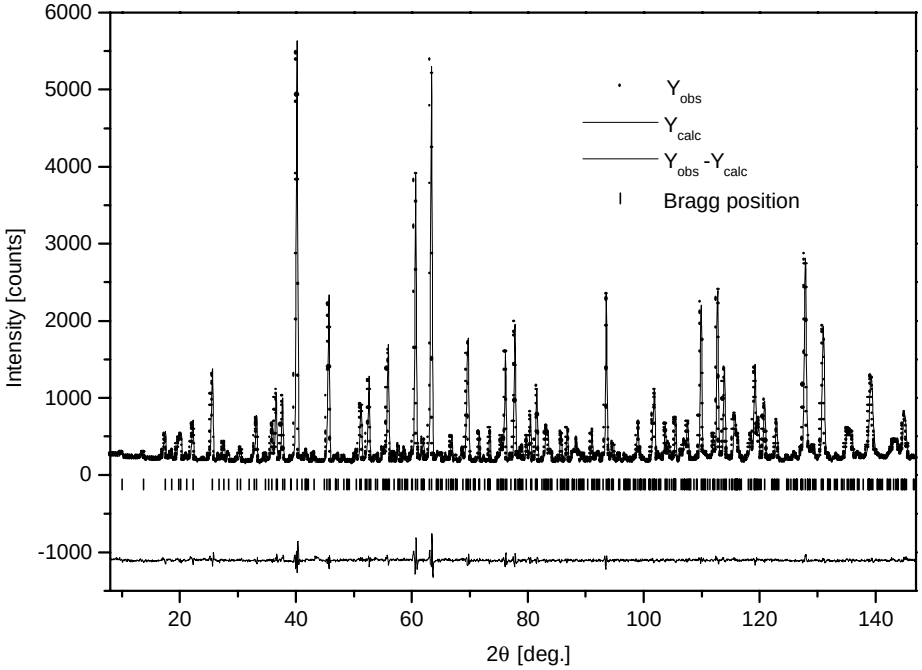

Fig. 4. Fitted neutron diffraction pattern for $Li_2ZnSn_3O_8$.

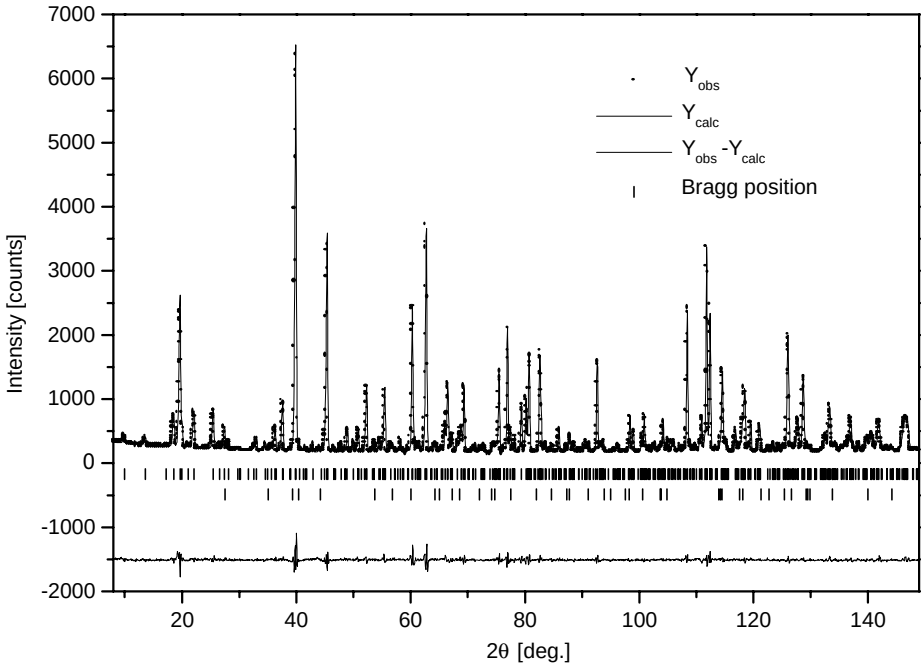

Fig. 5. Fitted neutron diffraction pattern of $Li_2MnSn_3O_8$. The lower set of Bragg positions belongs to 3.1 wt% SnO_2 impurity.

Table 3
Selected metal–oxygen distances (Å) and calculated valence sums for (a) $Li_2MnSn_3O_8$ and (b) $Li_2ZnSn_3O_8$

Central	Ligands						Average	Valence
(*a*) *$Li_2MnSn_3O_8$*								
Sn(1)	O(1)–2.18(1)	O(2)–2.03(1)	O(7)–2.04(2)	O(8)–2.00(1)	O(10)–2.15(2)	O(12)–2.03(2)	2.073(8)	3.87(8)
Sn(2)	O(3)–2.03(1)	O(4)–2.15(2)	O(6)–1.97(2)	O(9)–2.16(2)	O(11)–2.09(2)	O(14)–1.99(2)	2.064(8)	3.97(8)
Sn(3)	O(4)–2.15(2)	O(5)–2.03(2)	O(7)–2.03(2)	O(10)–2.14(2)	O(13)–2.04(2)	O(14)–2.03(2)	2.070(8)	3.88(9)
Li(1)	O(5)–2.23(2)	O(6)–2.15(2)	O(7)–2.13(3)	O(12)–2.15(2)	O(13)–2.26(2)	O(14)–2.02(2)	2.16(1)	0.94(2)
Li(2)	O(2)–2.15(2)	O(2)–2.15(2)	O(3)–2.12(3)	O(8)–2.05(3)	O(11)–2.24(2)	O(11)–2.24(2)	2.16(1)	0.93(3)
Li(3)	O(1)–2.10(3)	O(2)–1.92(2)	O(2)–1.92(2)	O(8)–1.92(3)			1.96(1)	1.06(6)
Li(4)	O(4)–2.37(2)	O(5)–1.90(2)	O(6)–1.94(2)	O(14)–1.86(2)			2.02(1)	1.02(4)
Mn(1)	O(3)–2.01(2)	O(9)–2.10(4)	O(10)–2.09(2)	O(10)–2.09(2)			2.07(1)	1.87(8)
Mn(2)	O(7)–2.06(1)	O(11)–2.04(2)	O(12)–1.99(3)	O(13)–2.01(4)			2.03(1)	2.12(9)
Sn(4)	O(1)–2.06(2)	O(4)–2.08(2)	O(4)–2.08(2)	O(9)–2.22(2)	O(11)–2.07(2)	O(11)–2.07(2)	2.10(9)	3.60(8)
Sn(5)	O(2)–2.06(2)	O(5)–2.03(2)	O(6)–2.01(2)	O(10)–2.18(2)	O(12)–2.13(2)	O(13)–2.10(2)	2.08(9)	3.74(9)
(*b*) *$Li_2ZnSn_3O_8$*								
Sn(1)	O(1)–2.13(2)	O(2)–1.98(2)	O(7)–2.02(2)	O(8)–2.03(1)	O(10)–2.19(2)	O(12)–2.06(2)	2.071(8)	3.93(8)
Sn(2)	O(3)–2.02(2)	O(4)–2.13(2)	O(6)–1.98(2)	O(9)–2.18(2)	O(11)–2.06(2)	O(14)–2.00(2)	2.061(8)	4.01(9)
Sn(3)	O(4)–2.18(2)	O(5)–2.04(2)	O(7)–2.03(2)	O(10)–2.15(2)	O(13)–2.05(2)	O(14)–1.99(2)	2.072(9)	3.88(10)
Li(1)	O(5)–2.16(4)	O(6)–2.14(3)	O(7)–2.09(4)	O(12)–2.14(4)	O(13)–2.25(3)	O(14)–2.00(3)	2.13(1)	1.08(4)[a]
Li(2)	O(2)–2.18(3)	O(2)–2.18(3)	O(3)–2.14(4)	O(8)–2.03(4)	O(11)–2.17(3)	O(11)–2.17(3)	2.15(1)	1.07(4)[a]
Li(3)	O(1)–2.19(4)	O(2)–1.82(2)	O(2)–1.82(2)	O(8)–1.86(4)			1.92(2)	1.26(5)
Li(4)	O(4)–2.36(3)	O(5)–1.91(3)	O(6)–1.96(3)	O(14)–1.81(3)			2.01(1)	1.04(4)
Zn(1)	O(3)–2.03(2)	O(9)–2.07(4)	O(10)–2.10(2)	O(10)–2.10(2)			2.03(1)	1.56(6)[a]
Zn(2)	O(7)–2.01(2)	O(11)–1.98(3)	O(12)–2.00(3)	O(13)–1.94(2)			1.98(1)	1.87(6)[a]
Sn(4)	O(1)–2.09(3)	O(4)–2.07(2)	O(4)–2.07(2)	O(9)–2.15(3)	O(11)–2.11(2)	O(11)–2.11(2)	2.10(1)	3.55(8)
Sn(5)	O(2)–2.05(2)	O(5)–2.00(3)	O(6)–2.02(3)	O(10)–2.19(2)	O(12)–2.14(3)	O(13)–2.05(2)	2.08(1)	3.84(11)

[a] Values calculated for mixed occupancy sites (see Table 2).

For both structures, the c/a ratio of the hexagonal subcell (1.616 for $Li_2MnSn_3O_8$ and 1.628 for $Li_2ZnSn_3O_8$) is smaller than the ideal value of 1.633 for the hexagonal close packing.

The new structure has the same polyhedral representation as that of the DH phase; with the only difference being that cations in the mixed [Oc_3] layers are ordered (see Fig. 6). Octahedra occupied by Sn(1), Sn(2) and

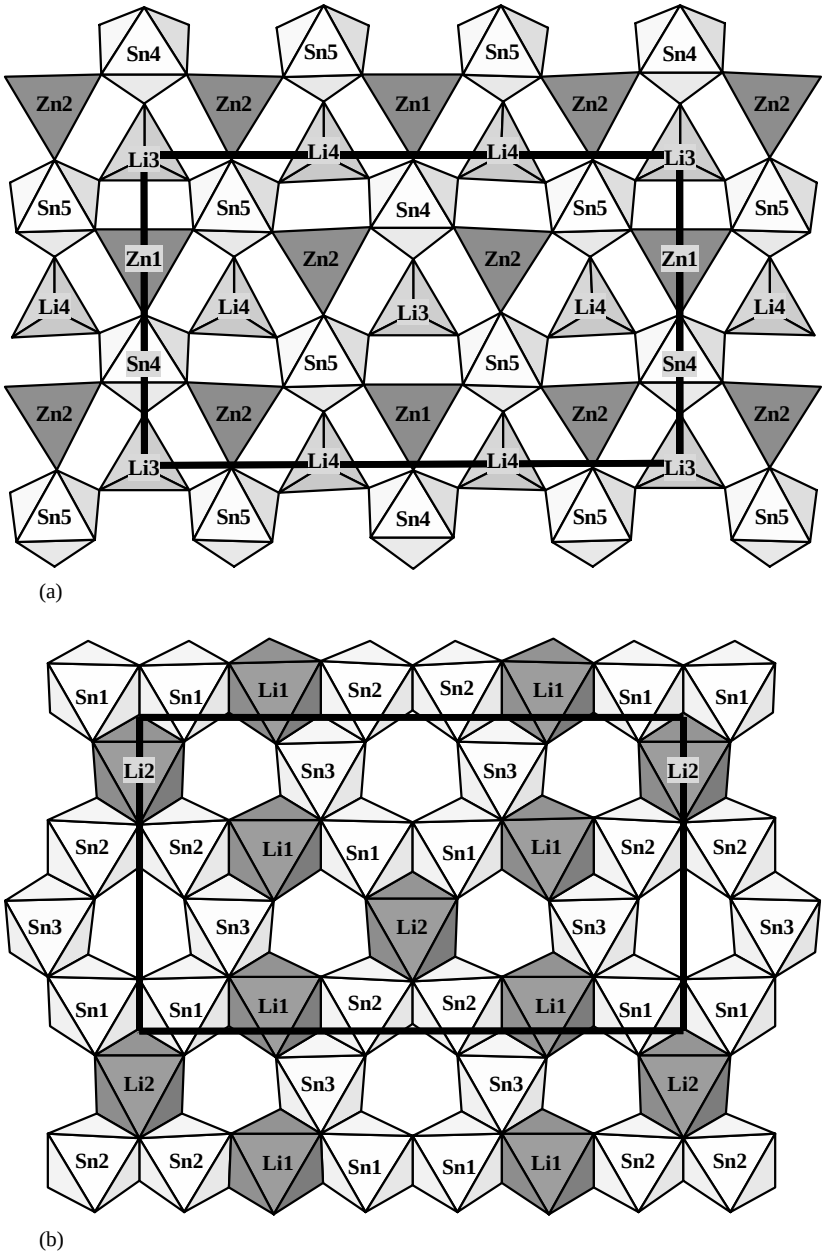

Fig. 6. Projection of the structure of $Li_2MSn_3O_8$ ($M = Zn, Mn$) along the c-axis. (a) [T_2Oc] layer and (b) [Oc_3] layer showing complete ordering of tin- and lithium-occupied octahedra. The unit cell is outlined.

Sn(3) form six-member isolated rings, linked together by six individual Li(1) and Li(2) occupied octahedra. The metal–oxygen interatomic distances (see Table 3) agree well with the corresponding ionic radii. The calculated BVS confirm the occupation of the particular lattice sites by individual ions. To our knowledge, such cation ordering in DH-type structures is reported for the first time.

The metal–metal distances are listed in Table 4. As can be seen, the Sn–Sn distances within the [Oc_3] layer are larger than those of Sn–Li within the same layer. This is an indication of the strong electrostatic repulsion between the high-valence ions, occupying the edge-sharing octahedra. These distances are higher than metal–metal distances reported for the phases with disordered [Oc_3] layers, and agree with the values observed in the SnO_2 (cassiterite) structure [12]. The large Sn–Sn distances within the [Oc_3] layers explain the smaller than ideal c/a ratio. The so-formed Kagomé layer has two types of holes, one surrounded by six SnO_6 octahedra and the other by three LiO_6 and three SnO_6 octahedra. The geometry of the [T_2Oc] layer is identical to that of the DH-phase. The octahedral holes in the [Oc_3] Kagomé layer are blocked by Sn^{4+} occupied octahedra and M^{2+} occupied tetrahedra, while the Li^+ occupied tetahedra link groups of three octahedra

Table 4
Octahedral metal–metal distances (Å) in $Li_2MnSn_3O_8$ and $Li_2ZnSn_3O_8$

Sample	$Li_2MnSn_3O_8$	$Li_2ZnSn_3O_8$
Distances within [Oc_3] *layers*		
Sn(1)–Sn(1)	3.22(2)	3.19(2)
Sn(1)–Sn(3)	3.17(1)	3.17(1)
Sn(2)–Sn(2)	3.15(1)	3.12(1)
Sn(2)–Sn(3)	3.16(1)	3.14(1)
Li(1)–Sn(1)	3.00(2)	2.94(3)
Li(1)–Sn(2)	3.00(2)	3.02(3)
Li(1)–Sn(3)	3.03(2), 3.02(2)	2.99(3), 2.97(3)
Li(2)–Sn(1)	2.99(2)	2.94(3)
Li(2)–Sn(3)	3.03(2)	3.00(3)
Distances between [Oc_3] *and* [T_2O] *layers*		
Sn(1)–Sn(5)	3.28(1)	3.30(2)
Sn(3)–Sn(5)	3.28(1)	3.25(2)
Sn(2)–Sn(4)	3.34(1)	3.29(2)
Li(1)–Sn(5)	3.24(2)	3.21(5)
Li(2)–Sn(4)	3.29(3)	3.21(5)

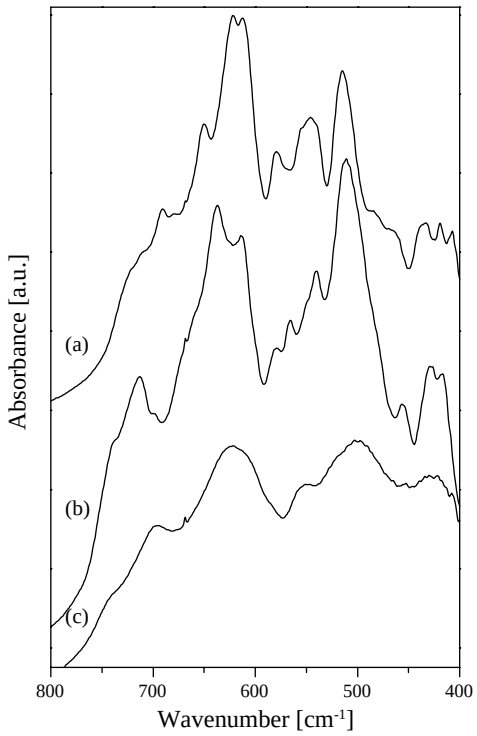

Fig. 7. Infrared spectra of (a) $Li_2MnSn_3O_8$, (b) $Li_2ZnSn_3O_8$ and (c) $Li_{1.6}Zn_{1.6}Sn_{2.8}O_8$.

(two occupied by Sn^{4+} and one by Li^+). In this case, the Sn(4) and Sn(5) octahedra of the [T_2Oc] layer have larger Sn–O distances on average, and, respectively, lower valence sums, compared to those of the Sn(1), Sn(2) and Sn(3) in the [Oc_3] layers. Although the mean values of the octahedral and tetrahedral bond lengths are in a good agreement with those reported in the literature [1–6], all coordination polyhedra are rather distorted.

The cation ordering and coordination polyhedron distortions can also be seen from the examination of the infrared spectra of the two compounds (Figs. 7a and b). The IR-spectra of $Li_2MnSn_3O_8$ and $Li_2ZnSn_3O_8$ are very complex and exhibit a relatively large number of sharp bands within the range 400–800 cm^{-1}. The two high intensive bands in the range 450–650 cm^{-1} can be attributed to the vibrations of the SnO_6 octahedra. Their splitting is in agreement with the presence of five crystallographically different octahedral positions for Sn^{4+} ions and with the different bond lengths between the cations and oxygen atoms. For comparison, we show on the same figure (Fig. 7c) the IR-spectrum of the DH-phase ($Li_{1.6}Zn_{1.6}Sn_{2.8}O_8$) which exhibits only a few relatively broad bands, as should be expected for compounds with mixed site occupancies [13].

There are at least two antagonistic factors, which play a role for the cation sub-lattice of the DH-type structure. The first is the electrostatic factor. From this point of view, the occupation of two adjacent, edge-chairing octahedra by high valence cations leads to an electrostatic repulsion and lattice instability. The second is the geometrical factor. From this aspect, the occupation of one site by ions with different ionic radii is unfavorable since it would introduce high local distortions. The balance between these two factors may depend on phase composition and synthesis conditions. The observed two-dimensional ordering in the [Oc_3] layer for $Li_2ZnSn_3O_8$ and $Li_2MnSn_3O_8$ indicates that for both compositions the second factor prevails over the first one. In this particular case, the difference between the octahedral ionic radii of Sn^{4+} (0.69) and Li^+ (0.76) seems to be dominant and leads to the expulsion of Li^+ from the mixed sites into the linking sites of the Kagomé layers. The same factor explains the ordering in Li_2SnO_3 and other $Li_2M^{4+}O_3$ structures [14]. The geometrical size factor seems to be responsible also for the cation ordering in spinel $Li_2MTi_3O_8$ ($M = Zn, Co$) [15], $Li_2MGe_3O_8$ [16] and $LiAl_5O_8$ [17], where the difference between the octahedral ionic radii of Li^+(0.76) on one hand and Ti^{4+}(0.605), Ge^{4+}(0.53) and Al^{3+}(0.535) on the other, is even more drastic. In all compounds, the octahedral sub-lattice splits. Titanium atoms occupy 12(*d*) and lithium ones—4(*b*) positions of the space group $P4_332$.

References

[1] J. Choisnet, B. Raveau, Mater. Res. Bull. 14 (1979) 1381.
[2] J. Choisnet, M. Hervieu, B. Raveau, P. Tarte, J. Solid State Chem. 40 (1981) 344.

[3] P. Tarte, R. Cahay, J. Preudhomme, M. Hervieu, J. Choisnet, B. Raveau, J. Solid State Chem. 44 (1982) 282.
[4] P. Lacorre, M. Hervieu, J. Pannetier, J. Choisnet, B. Raveau, J. Solid State Chem. 50 (1983) 196.
[5] P. Lacorre, M. Herviewu, J. Choisnet, B. Raveau, J. Solid State Chem. 51 (1984) 44.
[6] J. Choisnet, M. Hervieu, B. Raveau, P. Tarte, J. Solid State Chem. 45 (1982) 280.
[7] L. Dupont, M. Hervieu, G. Rousse, C. Masquelier, M.R. Palacin, Y. Chabre, J.M. Tarascon, J. Solid State Chem. 155 (2000) 394.
[8] J. Rodrigues-Carvajal, Physica B (Amsterdam) 192 (1993) 55.
[9] R. Franke, J. Rothe, R. Becker, J. Pollmann, J. Hormes, H. Bonnemann, W. Brijoux, R. Koppler, Adv. Mater. 10 (2) (1998) 126.
[10] M.A. Langell, C.W. Hutchings, A.G. Carson, M.H. Nassir, J. Vac. Sci. Technol. A 14 (3) (1996) 1656.
[11] R.D. Shannon, Acta Crystallogr. A 32 (1976) 751.
[12] A.A. Bolzan, C. Fong, B.J. Kennedy, C.J. Howard, Acta Crystallogr. B 53 (1997) 373.
[13] N. Chaban, N. Porotnikov, L. Margolin, K. Petrov, Russ. J. Inorg. Chem. [Engl. Transl.] 30 (1985) 1663.
[14] J.L. Hodeau, M. Marezio, A. Santoro, R.S. Roth, J. Solid State Chem. 45 (1982) 170.
[15] J.-C. Joubert, A. Durif-Varambon, Bull. Soc. Franc. Miner. Crist. 86 (1963) 92.
[16] K. Hirota, M. Ohtani, N. Mochida, A. Ohtsuka, Nippon Seram. 96 (1988) 92.
[17] M. Krieus, G. Adiwidjaja, W. Guse, K.H. Klaska, C. Lathe, H. Saalfeld, Neues Jahrb. Mineral. 1996 (1996) 334.